Molecular Crystals and Liquid Crystals Science and Technology. Section A. Molecular Crystals and Liquid Crystals

Publication details, including instructions for authors and subscription information:
http://www.tandfonline.com/loi/gmcl19

Macroscopic Properties of Ferronematics Caused by Orientational Interactions on the Particle Surfaces. II. Behavior of Real Ferronematics in External Fields

Sergei V. Burylov [a] & Yuri L. Raikher [b]

[a] Transmag Research Institute, Ukrainian Academy of Sciences, Dnepropetrovsk, 320005, Ukraine

[b] Institute of Continuous Media Mechanics, Urals Branch of the Russian Academy of Sciences, Perm, 614061, Russia

Version of record first published: 23 Sep 2006.

To cite this article: Sergei V. Burylov & Yuri L. Raikher (1995): Macroscopic Properties of Ferronematics Caused by Orientational Interactions on the Particle Surfaces. II. Behavior of Real Ferronematics in External Fields, Molecular Crystals and Liquid Crystals Science and Technology. Section A. Molecular Crystals and Liquid Crystals, 258:1, 123-141

To link to this article: http://dx.doi.org/10.1080/10587259508034553

Mol. Cryst. Liq. Cryst., 1995, Vol. 258, pp. 123–141
Reprints available directly from the publisher
Photocopying permitted by license only

Macroscopic Properties of Ferronematics Caused by Orientational Interactions on the Particle Surfaces. II. Behavior of Real Ferronematics in External Fields

SERGEI V. BURYLOV

Transmag Research Institute, Ukrainian Academy of Sciences, Dnepropetrovsk, 320005, Ukraine

YURI L. RAIKHER

Institute of Continuous Media Mechanics, Urals Branch of the Russian Academy of Sciences, Perm, 614061, Russia

(Received Nov. 8, 1993; in final form April 20, 1994)

On the basis of the worked out modification of the continuum theory of ferronematics the Fredericksz transitions and orientational birefringence induced by magnetic and/or electric field are studied. A comparison with the available experimental data is made.

Keywords: Liquid-crystalline suspension, finite anchoring, ferronematics, electric birefringence, magnetic birefringence

PACS numbers: 61.30.Gd 75.50.Mm 82.70.Kj

INTRODUCTION

In the first part[1] of this paper we have in detail presented a modified approach to the continuum theory of ferronematics (FN), i.e., suspensions of fine magnetic particles in nematic liquid-crystalline carriers. The essential feature of this modification is an assumption that the anchoring energy of the nematic molecules on the particle surfaces is finite. Moreover, it turned out that for real thermotropic FN like those studied in Refs. [2, 3, 4] the characteristic ratio

$$\omega = WR/K, \tag{1}$$

where W is the anisotropic part of the surface energy density for the particle-nematic interface, K is the orientational-elastic (Frank) modulus and R the reference size of the particle, is less than unity. Using ω from Equation (1) as the expansion parameter, we have shown[1,5] that for FN with homeotropic anchoring and $\omega < 1$ the basic state is

the one where the average orientation $\boldsymbol{n}$ and magnetization $\boldsymbol{M}$ are mutually perpendicular. The expression for the free-energy density for FN with $\omega < 1$ and any type of boundary condition, derived in Ref. [1], reads

$$F = 1/2\ [K_1(\mathrm{div}\,\boldsymbol{n})^2 + K_2(\boldsymbol{n}\cdot\mathrm{curl}\,\boldsymbol{n})^2 + K_3(\boldsymbol{n}\times\mathrm{curl}\,\boldsymbol{n})^2] - 1/2\ \chi_a(\boldsymbol{nH})^2$$

$$- M_s f(\boldsymbol{mH}) + (f k_B T/v)\ln f + (AWf/d)(\boldsymbol{nm})^2. \tag{2}$$

Here X_a is the anisotropic part of the diamagnetic susceptibility of nematic, $\boldsymbol{H}$ is the external field, M_s is the saturation magnetization of the particle substance, d and v are the diameter of a rod-like particle and its volume, respectively, $\boldsymbol{m}$ is the unit vector of the FN magnetization direction defined as $\boldsymbol{M} = M_s f\boldsymbol{m}$ and f is the volume fraction of the particles. Coefficient $A = 1 - 3\cos^2\alpha$ characterizes the type of the boundary condition, where α is the easy-orientation angle of the nematic director $\boldsymbol{n}$ on the particle surface; for homeotropic anchoring A is positive and equals to unity.

In the following we apply our model[1] to the orientational behavior of FN with the homeotropic soft ($A = 1$, $\omega < 1$) anchoring and use the results to interpret the experimental data on real thermotropic FN reported in a series of papers.[2-4] While considering the FN layers, we take for granted that in the initial unperturbed state the sample (*i*) consists of a single liquid-crystalline domain and (*ii*) is subjected to a permanent bias field $\boldsymbol{H}_b \perp \boldsymbol{n}_0$ due to which is magnetized up to saturation with $\boldsymbol{M}_0 = M_s f\boldsymbol{m}_0$ along the direction of $\boldsymbol{H}_b$. The first of these assumptions is a usual idealization to avoid taking into account the liquid-crystalline defects of non-magnetic origin. The second one, as it is shown in Ref. [1], is necessary both in theory and experiment to remove the orientational degeneracy of the particle magnetic moments which occurs in the "easy-plane" structures where $\boldsymbol{M}_0$ is perpendicular to $\boldsymbol{n}_0$. In the above-used notations, as well as in below, the subscript 0 refers to the orientational variables describing the initial state of the sample which is supposed to be spatially uniform.

1 MAGNETIC BIREFRINGENCE IN FERRONEMATICS

1.1 Derivation of the formula for the optical phase lag

In our recent paper[6] we have given an example, how the presence of magnetic particles modifies the classical liquid-crystalline effect—the diamagnetic Fredericksz transition—in FN. In below we address the phenomena of another type—the field-induced effects which are exclusively inherent to FN and are provoked by magnetic fields whose order of magnitude does not exceed 10 Oe. Apparently, in fields so weak, the diamagnetic term in Equation (2) is insignificant and thus may be omitted.

Consider a magneto-optical effect in the orientational structure presented in Figure 1. Homeotropic FN cell is subjected to a constant external field having two components: $\boldsymbol{H}$ and $\boldsymbol{H}_b$, respectively, parallel and normal to the unperturbed director $\boldsymbol{n}_0$. According to the proposed in Ref. [1] concept of magnetization of FN with soft anchoring, we assume that small bias field $H_b \sim 1$ Oe is imposed and fixed once and forever, while the value of H might change arbitrarily. In the initial state, that is at

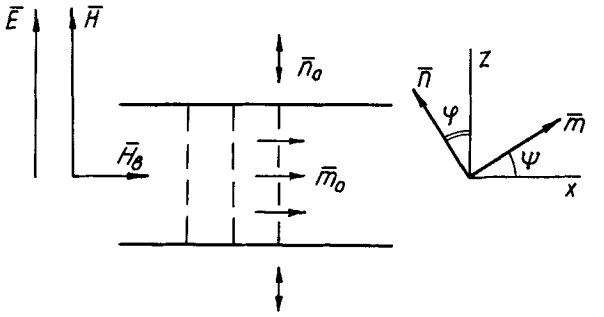

FIGURE 1 A flat layer of a ferronematic in the external magnetic field $\boldsymbol{H}_p = \boldsymbol{H} + \boldsymbol{H}_b$; in the right-hand part the choice of the coordinate axes and reference angles is shown. The electric field $\boldsymbol{E}$ is present only for the case considered in Sec. 3.

$H = 0$, the ferromagnetic admixture is homogeneously distributed over the cell volume and the sample is uniformly magnetized up to saturation $M_0 = M_s \bar{f}$ in the direction of $\boldsymbol{H}_b$.

Distortions induced by the field $\boldsymbol{H} + \boldsymbol{H}_b$ are characterized by two orientational distributions

$$\boldsymbol{n} = (-\sin\varphi(z), 0, \cos\varphi(z)), \quad \boldsymbol{m} = (\cos\psi(z), 0, \sin\psi(z)); \tag{3}$$

the choice of the angles and coordinate axes is shown in the right-hand side of Figure 1. This texture is birefringent for any light beam propagating along the z-axis. The optical phase lag between the extraordinary (refraction index n_e) and ordinary (n_o) rays is given by formula

$$\delta = \frac{2\pi}{\lambda_{light}} \int_{-D/2}^{D/2} (n - n_o)\, dz, \tag{4}$$

where λ_{light} is the wavelength of the light in an empty space, D is the cell thickness and $n = n(z)$ is the effective refraction index defined as

$$n^{-2}(z) = n_o^{-2}\cos^2\varphi(z) + n_e^{-2}\sin^2\varphi(z).$$

Let us derive a set of equations describing the equilibrium state of FN at given $\boldsymbol{H}$ and evaluate the dependence $\delta(H)$. The expression for the free-energy functional $\mathscr{F}$ is obtained by integration of Equation (2) across the cell, with Equation (3) substituted therein. This yields

$$\mathscr{F} = \int_{-D/2}^{D/2} dz \Big[1/2\, K_3\, \varphi'^2 (1 + p\sin^2\varphi) - M_s f(H_b\cos\psi + H\sin\psi)$$

$$+ \frac{fW}{d}\sin^2(\psi - \varphi) + \frac{fk_BT}{v}\ln f \Big]. \tag{5}$$

Here we have introduced a dimensionless parameter $p = (K_1 - K_3)/K_3$, and use the prime to denote differentiation with respect to z. As it is apparent, $\mathcal{F}$ depends upon three functions: angular distributions $\varphi(z)$ and $\psi(z)$ and concentration $f(z)$; the sought for equilibrium equations are delivered by corresponding variations of $\mathcal{F}$. The first of them ($\delta\mathcal{F}/\delta\varphi = 0$) yields

$$\varphi''(1 + p\sin^2\varphi) + \varphi'^2 p\sin\varphi\cos\varphi + (fW/K_3 d)\sin 2(\psi - \varphi) = 0. \tag{6}$$

The second ($\delta\mathcal{F}/\delta\psi = 0$) has the meaning of the bonding equation—see [1, Sec. **6**]—and assumes the form

$$M_s(H_b\sin\psi - H\cos\psi) + (W/d)\sin 2(\psi - \varphi) = 0. \tag{7}$$

The third one ($\delta\mathcal{F}/\delta f = 0$) accounts for the seggregation effect—see [1, Sec. **6**], and reads

$$f = \bar{f}Q\mathcal{E}(\psi,\varphi), \quad Q = D\left[\int_{-D/2}^{D/2} \mathcal{E}(\psi,\varphi)\,dz\right]^{-1}, \tag{8}$$

where

$$\mathcal{E}(\psi,\varphi) = \exp\left[\rho_b\cos\psi + \rho\sin\psi - \sigma\sin^2(\psi - \varphi)\right];$$

and the scaled by temperature dimensionless parameters are

$$\rho_b = M_s v H_b/k_B T, \quad \rho = M_s v H/k_B T, \quad \sigma = Wv/k_B T d.$$

As the first step to solve the set (6)–(8), we multiply Equation (6) by φ', Equation (7) by $f\psi'$ and subtract the latter from the former simultaneously substituting f from Equation (8). In result we arrive at the integro-differential equation

$$K_3\varphi'\left[\varphi''(1 + p\sin^2\varphi) + p\varphi'^2\sin\varphi\cos\varphi\right] + (\bar{f}QW/d)\mathcal{E}(\psi,\varphi)(\psi' - \varphi')$$
$$\cdot\sin 2(\psi - \varphi) + M_s\bar{f}Q\psi'\mathcal{E}(\psi,\varphi)(H\cos\psi - H_b\sin\psi) = 0. \tag{9}$$

Together with the bonding equation (7) it determines, albeit implicitly, the orientational distributions $\varphi(z)$ and $\psi(z)$.

As it has been explained in Ref. [6], for sufficiently thick layers the difference between soft and rigid anchoring of nematic at the cell wall is irrelevant, and we may as well impose rigid boundary conditions on φ. It is natural to anticipate that in the middle

plane of the layer the angular deviations are maximum. So, for the orientational profile we set

$$\varphi(\pm D/2) = 0, \quad \varphi'(0) = 0. \tag{10}$$

For Equation (9) the first integral is available. With the aid of the second of the conditions (10) it may be written as

$$\lambda^2 \varphi'^2 (1 + p\sin^2\varphi) - Q\,[\mathscr{E}(\psi_m, \varphi_m) - \mathscr{E}(\psi, \varphi)] = 0. \tag{11}$$

Here the angles $\varphi_m \equiv \varphi(0)$ and $\psi_m \equiv \psi(0)$, connected by Equation (7), describe the angular positions of the director and the magnetization vectors in the middle plane of the cell. The length parameter $\lambda = (K_3 v/2\bar{f} k_B T)^{1/2}$ determines the distance by which the orienting influence of the wall penetrates into a semi-infinite FN sample in a sufficiently strong magnetic field.[7,8]

Resolving Equation (11) for dz, one finds

$$dz = \mp \lambda Q^{-1/2} (1 + p\sin^2\varphi)^{1/2} [\mathscr{E}(\psi_m, \varphi_m) - \mathscr{E}(\psi, \varphi)]^{-1/2}\, d\varphi; \tag{12}$$

here the signs $\mp$ refer to the upper and lower half-spaces, respectively—see Figure 1. Integration of Equation (12) at $z > 0$ with allowance for Equations (10) yields

$$(D - 2z)/\lambda = 2\varphi^{-1/2} I(\varphi), \tag{13}$$

where

$$I(\varphi) = \int_0^{\varphi} (1 + p\sin^2 t)^{1/2} [\mathscr{E}(\psi_m, \varphi_m) - \mathscr{E}(\psi(t), t]^{-1/2}\, dt.$$

In the plane $z = 0$, where $\varphi = \varphi_m$, Equation (13) transforms into equality

$$D/\lambda = 2Q^{-1/2} I(\varphi_m), \tag{14}$$

that enables to eliminate the coefficient Q and rearrange Equation (13) as

$$1 - 2z/D = I(\varphi)/I(\varphi_m). \tag{15}$$

The last relation and the bonding equation (7) that could be rewritten in the form

$$\rho_b \sin\psi - \rho\cos\psi + \sigma\sin 2(\psi - \varphi) = 0, \tag{16}$$

make a closed subset determining the orientational dependences $\varphi(z)$ and $\psi(z)$ at given φ_m. Using Equation (12) to change the variables in Equation (8), we find

$$Q = I(\varphi_m)/J(\varphi_m), \tag{17}$$

where

$$J(\varphi) = \int_0^{\varphi} (1 + p\sin^2 t)^{1/2} \mathscr{E}(\psi(t), t) [\mathscr{E}(\psi_m, \varphi_m) - \mathscr{E}(\psi(t), t]^{-1/2} dt.$$

Substitution of Equation (17) into Equation (14) gives

$$(D/2\lambda)^2 = I(\varphi_m) \cdot J(\varphi_m), \tag{18}$$

that completes the full set of equations comprising now Equations (15)–(18).

To evaluate the experimentally observed function $\delta(H)$, we transform Equation (4) with the aid of Equation (12) and Equation (15), thus arriving at the formula

$$\delta = \frac{2\pi n_o D}{\lambda_{light} I(\varphi_m)} \int_0^{\varphi_m} \left[n_e (n_e^2 \cos^2 t + n_o^2 \sin^2 t)^{-1/2} - 1 \right] (1 + p\sin^2 t)^{1/2}$$

$$\times [\mathscr{E}(\psi_m, \varphi_m) - \mathscr{E}(\psi(t), t)]^{-1/2} dt, \tag{19}$$

determining the phase lag between the ordinary and extraordinary rays in a deformed by field $\boldsymbol{H}$ texture of FN.

1.2 Interpretation of the experiment

The results of numerical evaluation of the theoretical dependence $\delta^{1/2}(H)$ given by Equation (19) for a number of cell thicknesses and particle concentrations are presented in Figures 2 and 3. Various dots are the experimental data reported in Ref. [2] for the birefringence of flat FN cells. These observations were performed at room temperature, the initial orientation pattern corresponded to that sketched in Figure 1. The carrier of FN was made of the well-known liquid crystal MBBA, whose elastic moduli are $K_1 \approx 5 \cdot 10^{-7}$ dyn and $K_3 \approx 8 \cdot 10^{-7}$ dyn according to Ref. [9]. The wavelength of the laser light beam was $\lambda_{light} = 6.328 \cdot 10^{-5}$ cm; for the refraction indices of MBBA, after,[10] we set $n_o \approx 1.5$ and $n_e \approx 1.7$. The role of $\boldsymbol{H}_b$ in Ref. [2] was played by the terrestrial magnetic field; its strength in our calculations we have set to 0.6 Oe. For the given particle size: length $L \approx 5 \cdot 10^{-5}$ cm and diameter $d \approx 7 \cdot 10^{-6}$ cm, this bias field yields $\rho_b = 10$. For the amplitude W of the anisotropic part of the anchoring energy (the particles were coated with the DMOAP surfactant—see Ref. [2]) we took $5 \cdot 10^{-2}$ dyn/cm.

The most difficult item in the undertaken experiment interpretation is to estimate the particle concentration. Indeed, while FN preparation there occurs a partial coagulation of the magnetic grains, i.e., formation of large multi-particle aggregates. Since such objects have a closed configuration of constituting magnetic moments, their net moment is next to zero. Due to that the aggregates become insensitive to the action of weak external fields thus passing away for the considered birefringence effect. In

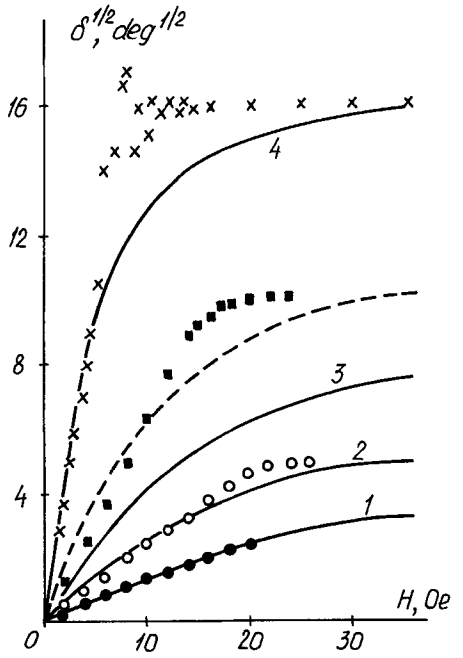

FIGURE 2 Field-strength dependences of the optical phase lag for different thicknesses D of the FN cell. The assumed initial concentration of single-domain ferroparticles $\bar{f} = 1.12 \cdot 10^{-6}$; the given in Ref. [2,3] total one evaluated by weight measurement is $\bar{f} = 2.98 \cdot 10^{-6}$; the lines–theory, the dots–experimental data by Ref. [2]; $D = 123$ μm (curve *1* and black circles), 152 μm (*2* and empty circles), 189 μm (*3* and squares), 354 μm (*4* and crosses). The dashed line (cf. curve *3*) is the theoretical curve for $D = 189$ μm at $\bar{f} = 2.0 \cdot 10^{-6}$.

result, the volume fraction of the particles, which really impart strong magneto-optical response to FN, should reduce substantially in comparison with the total solid phase content of the suspension.

Let us show how a reasonable estimation for the true concentration of single-domain particles might be found from the experimental data plotted in Figures 2, 3. Consider the response of the liquid-crystalline suspension in an extremely weak magnetic field $H < H_b$, i.e. $\rho < \rho_b < \sigma$. In this case Equation (16) allows to treat the local bonding of the orientational distributions $\boldsymbol{n}(z)$ and $\boldsymbol{m}(z)$ as rigid: $\psi(z) = \varphi(z)$, i.e., $\boldsymbol{n} \perp \boldsymbol{m}$—see Figure 1. Solving the properly simplified Equations (15) and (18), one finds that at $\rho\varphi_m \ll 1$ function $\varphi(z)$ acquires a parabolic profile

$$\varphi(z) = (M_s \bar{f} H D^2 / 8 K_3)[1 - 4z^2/D^2].$$

Substituting this into the integral (19), for the phase lag in the $\rho\varphi_m \ll 1$ range, one gets

$$\delta^{1/2}(H) = \left[\pi D^5 (n_e - n_0)/60 \lambda_{light}\right]^{1/2} (M_s \bar{f} H / K_3). \tag{20}$$

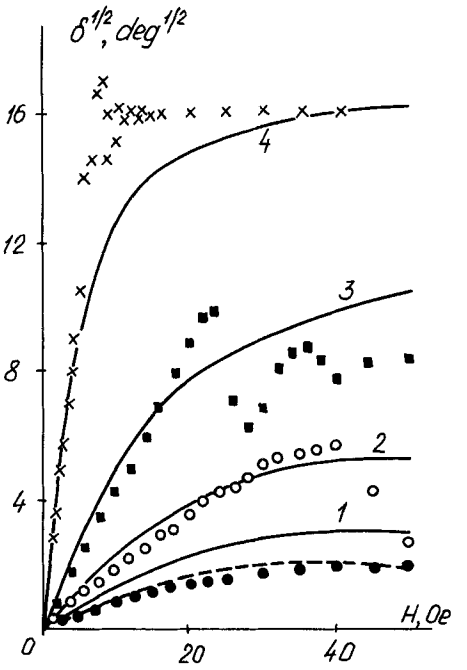

FIGURE 3 Field-strength dependence of the optical phase lag for different concentrations of single-domain ferroparticles at $D = 354\,\mu m$ (curves *1*, *3*, *4*) and $D = 337\,\mu m$ (curve *2*). The lines–theory, the dots–experimental data by Ref. [2]; $f = \bar{f}_m = 7 \cdot 10^{-8}$ (*1* and black circles), $2\bar{f}_m$ (*2* and empty circles), $4\bar{f}_m$ (*3* and squares), $16\bar{f}_m$ (*4* and crosses). The dashed line (cf. curve *1*) is the theoretical curve for $\bar{f} = 5 \cdot 10^{-8}$.

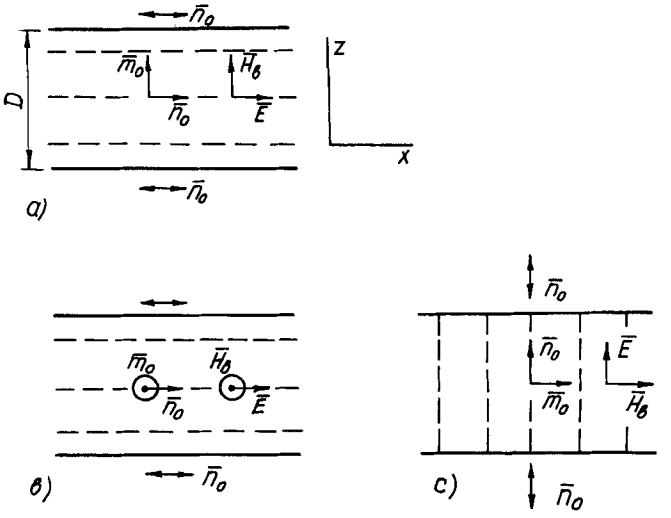

FIGURE 4 Initial textures of the FN cells with planar (*a* and *b*) and homeotropic (*c*) anchoring, where the dielectric Fredericksz transition takes place.

This expression proves that in weak fields function $\delta^{1/2}$ is linear in the field-strength and its initial slope is directly proportional to the sought for magnetic admixture concentration $\bar{f}$ not yet spoiled by the seggregation effect. In our interpretation we deduce the true value $\bar{f}$ applying formula (20) to the initial regions of the experimental curves. The reference (lowest) concentration $\bar{f}_m$ by which the volume fraction $\bar{f}$ is scaled in Figures 2, 3, has been evaluated from the line *2* in Figure 3; the result is $\bar{f}_m = 7{\cdot}10^{-8}$. Further on, this very value, being about 40% of the total solid phase amount $1.86{\cdot}10^{-7}$ reported in Ref. [2], had been used in the fitting procedures for all the other theoretical curves (solid lines) plotted in Figures 2, 3. We dare to speculate that for two particular experiments, corresponding to curve *3* of Figure 2 and curve *1* of Figure 3, the normalizing factor $\bar{f}_m$ has somehow deviated considerably from the cited $\bar{f}_m$ value. This assumption is confirmed by the results of re-calculation (dashed lines in Figures 2, 3) with the changed values of $\bar{f}$.

In their general features, the obtained theoretical dependences based on Equation (19) agree with the experimental data. In weak fields the dots reasonably comply with the linear function (20). Further growth of the birefringence $\delta^{1/2}(H)$ is more slow in comparison with the linear law, and in the $H \sim 20$–40 Oe range both theoretical and experimental graphs show the optical saturation of FN. The observed oscillations of $\delta^{1/2}(H)$ in some curves are most probably, as it has already been mentioned in Ref. [2], caused by the coagulation of ferroparticles. Apparently, in a dilute system coagulation of ferroparticles is the direct result of the seggregation effect. The latter provokes the re-distribution of the particles even in rather weak fields. In particular, at $\rho\varphi_m \ll 1$ from Equations (8) and (7) it follows

$$f(z) = \bar{f}\left[1 + \rho^2 D^2\left(1 - 12z^2/D^2\right)\Big/ 48\lambda^2\right], \tag{21}$$

that means that the particles, minimizing their orientational energy, accumulate in the middle of the cell. The numerical calculations show that with H growing, the stratification of the magnetic admixture intensifies. At certain critical concentration the magnetic dipole–dipole interaction should lead to the abrupt local coagulation. Because of that, the fraction of isolated (single) particles reduces, and the observed birefringence falls down. However, the external field continues to grow, increasing the alignment and, hence, birefringence of the remained particles. Simultaneoulsy, seggregation pumps up new portions of particles into the middle of the cell. Due to that in this region the concentration grows anew until it once more achieves the critical value. Assuming such a sequence of coagulation cycles one gets a reasonable qualitative explanation of the observed oscillations of the optical response (see squares and crosses in Figs. 2,3).

2 ELECTRIC FREDERICKSZ TRANSITION IN A FERRONEMATIC

2.1 The transition thresholds

Here we study the effect of the bias magnetic field upon the electric Fredericksz transition in a ferronematic. It is worth to remind that actually it is just this electric

instability that is employed in the majority of the liquid-crystalline devices destined for image processing.

Consider the uniform FN textures presented in Figure 4. We assume that inside the cell there exists a constant bias field $\boldsymbol{H}_b \perp \boldsymbol{n}_0$ providing saturated uniform magnetization in the initial state. To take into account the dielectric properties of the liquid-crystalline matrix, one should include into the free-energy density expression (2) the term

$$F_{electr} = -\frac{\varepsilon_a}{8\pi}(\boldsymbol{n}\boldsymbol{E})^2. \tag{22}$$

Bearing in mind a MBBA-based ferronematic, we assume that the dielectric permeability anisotropy ε_a is negative. Then it is natural to expect that the instability of the uniform texture would be provoked by an electric field $\boldsymbol{E} \| \boldsymbol{n}_0$. Let us find the Fredericksz transition threshold for the cell with the configuration of Figure 4a. While performing the calculation, we will retain in F the diamagnetic contribution caused by the bias field.

Choosing the orientational perturbation of $\boldsymbol{n}$ and $\boldsymbol{m}$ in the form

$$\boldsymbol{n} = (1, n_y(z), n_z(z)), \quad \boldsymbol{m} = (m_x(z), m_y(z), 1), \quad f = \bar{f} + \delta f, \tag{23}$$

where n_y, n_z, m_x, m_y, and $\delta f/\bar{f}$ are small comparing to unity, with the accuracy up to the second power in small quantities one finds for the free energy functional

$$\delta\mathcal{F} = \frac{1}{2}\int_0^D dz\left[K_1\left(\frac{\partial n_z}{\partial z}\right)^2 + K_2\left(\frac{\partial n_y}{\partial z}\right)^2 + \frac{2\bar{f}W}{d}(m_x + n_z)^2\right.$$

$$\left. + M_s\bar{f}H_b m_x^2 - \chi_a H_b^2 n_z^2 + \gamma_a E^2\left(n_y^2 + n_z^2\right)\right]. \tag{24}$$

Here we have omitted the insignificant terms connected with m_y and δf, and introduced the notation $\gamma_a = \varepsilon_a/4\pi$. Evaluating, as in Ref. [6], the line of the steepest descent to the stability threshold by condition $(\delta/\delta m_x)\,\delta\mathcal{F} = 0$, we arrive at the relation

$$m_x = -n_z(1 + M_s Hd/2W)^{-1}, \tag{25}$$

and use it to eliminate m_x from Equation (24). With allowance for the rigid anchoring conditions $\boldsymbol{n}(0) = \boldsymbol{n}(D) = \boldsymbol{n}_0$ on the cell walls, the Fourier transformations

$$n_y = \sum_{k=1}^{\infty} \eta_k \sin\left(\frac{\pi k z}{D}\right), \qquad n_z = \sum_{k=1}^{\infty} \nu_k \sin\left(\frac{\pi k z}{D}\right)$$

reduce $\delta\mathscr{F}$ to the diagonal form. Integration across the cell yields

$$\delta\mathscr{F} = \frac{D}{4}\sum_{k=1}^{\infty}\left\{K_1\left(\frac{\pi k}{D}\right)^2 + \chi_a[G^2(H_b) - H_b^2] - |\gamma_a|E^2\right\}v_k^2$$

$$+\frac{D}{4}\sum_{k=1}^{\infty}\left\{K_2\left(\frac{\pi k}{D}\right)^2 - |\gamma_a|E^2\right\}\eta_k^2, \tag{26}$$

where function $G(H_b)$ is defined by formula

$$\tilde{H}_c^2 = H_c^2 + G^2(\tilde{H}_c), \qquad G(H) \equiv \left[\frac{2Wf\bar{M}_s H}{\chi_a(2W + M_s H d}\right]^{1/2}, \tag{27}$$

determining the Fredericksz transition threshold $\tilde{H}_c$ in FN; here $H_c = (\pi/D)(K_1/\chi_a)^{1/2}$ is the critical field value in a pure nematic. The solution is easy, because at $H \sim 10^2$ Oe there exists the small parameter $W/M_s H d \ll 1$; in the first order in it, Equation (27) transforms into

$$\tilde{H}_c^2 = H_c^2 + G^2, \quad G = G(\infty) = (2W\bar{f}/\chi_a d)^{1/2}, \tag{28}$$

The calculations for the textures in Figures 4 b,c give the same result save that for the pattern b moduli K_1 and K_2 in Equation (26) should interchange their places, and for the pattern c, where the instability is induced by the bend mode, only K_3, instead of K_1 and K_2, enters the expression for $\mathscr{F}$.

In the latter case the stability analysis is he most simple one. Indeed, for the critical electric field form Equation (26) at $K_i = K_3$ we find the set of equalities

$$\tilde{E}_c = \frac{1}{D|\gamma_a|^{1/2}}\begin{cases}(\pi^2 K_3)^{1/2}, \\ (\pi^2 K_3 + \chi_a D\Lambda)^{1/2},\end{cases} \tag{29}$$

where

$$\Lambda = G^2(H_b) - H_b^2.$$

It is apparent, that the observed value $\tilde{E}_c$ of the threshold corresponds to the smaller right-hand side of Equation (29). That means that we should find out the sign of function $\Lambda(H_b)$. Using Equation (28), it is easy to show that for $H_b < G = (2\bar{f}W/\chi_a d)^{1/2}$ this quantity is positive, i.e., the bias field stabilizes FN against the perturbations of n_z. In this case the Fredericksz transition threshold remains the same as in a pure nematic [9]:

$$\tilde{E}_c = E_c = (\pi/D)(K_3/|\gamma_a|)^{1/2}.$$

In the fields $G < H_b < \tilde{H}_c$ the diminution of the critical electric field, accounting for the growth of the destabilizing influence of the magnetic field H_b on the liquid-crystalline

matrix, takes place—see the results of Ref. [6]. Then the dependence $\tilde{E}_c(H_b)$ is given by the lower line of formula (29).

Now we return to consideration of the electric Fredericksz transition in the texture of Figure 4a. In this case the expressions for the critical field-strength read

$$\tilde{E}_c = \frac{1}{D|\gamma_a|^{1/2}} \begin{cases} (\pi^2 K_2)^{1/2} \\ (\pi^2 K_1 + \chi_a D\Lambda)^{1/2}, \end{cases} \tag{30}$$

and for a liquid crystal like MBBA or PAA one may set $K_1 \approx 2K_2$.[9] Deducing the condition under which the bias field diminishes the threshold of the transition in the electric field, we get

$$H_b^2 - G^2(H_b) > (\pi/D)^2 (K_1 - K_2)/\chi_a \approx (\pi/D)^2 (K_2/\chi_a),$$

which with allowance for Equation (28) transforms into

$$(\pi/D)^2 (K_2/\chi_a) + G^2 < H_b^2 < (\pi/D)^2 (K_1/\chi_a) + G^2.$$

For the texture of Figure 4b, where the critical field is determined similarly to Equation (30), save the replacement $K_1 \leftrightarrow K_2$, the calculation shows that inside the whole available magnetic field range the Fredericksz transition threshold is given by expression

$$\tilde{E}_c = \frac{1}{D}\left(\frac{\pi^2 K_2 + \chi_a \Lambda D^2}{|\gamma_a|}\right)^{1/2}.$$

2.2 Texture of a ferronematic above the threshold. Comparison with the experiment

The results of observation of the Fredericksz effect in thermotropic FN are reported in Ref. [3]. The studied textures corresponded to the one of Figure 4c; the suspension was magnetized by the terrestrial magnetic field. The critical electric potential difference $\tilde{V}_c = \tilde{E}_c D$ between the cell walls was determined optically by the onset of birefringence for the light beam directed along the z-axis. The dependence $\delta(\tilde{V})$ rendering the phase lag between the ordinary and extraordinary rays in the above-threshold range, i.e., for $\tilde{V} = ED > \tilde{V}_c$, has been measured. Let us calculate $\delta(\tilde{V})$ on the basis of the given theory, and compare it with the experimental data of Ref. [3].

As it follows from the results of Sec. **2.1**, in the configuration of Figure 4c at $H_b \sim 1$ Oe $< G$ the critical field-strength $\tilde{E}_c$ coincides (see Eqs. (29)) with that of a pure nematic. Apparently, in the electric field $E > \tilde{E}_c = E_c$ the minimum of the free-energy of the deformed FN corresponds to the state where the local director $\boldsymbol{n}$ lies in the yOz plane. At such a distortion the magnetic particles retain the initial orientation along $\boldsymbol{H}_b$ and remain normal to $\boldsymbol{n}$ all over the bulk of the cell. Due to that, the considered deformation of $\boldsymbol{n}$ does not invoke the change of the particle orientation energy. The equilibrium director distributions above the Fredericksz transition are exactly the same in pure nematic and in FN.

In the single-constant approximation $K_1 = K_2 = K_3 = K$ the function $\varphi(z)$ rendering the angular deviations $\boldsymbol{n}(z)$ from the direction of the initial orientation $\boldsymbol{n}_0$ for $0 \leqslant z \leqslant D/2$ is defined (see Ref. [9]) by equation

$$z = \xi_{electr} F(\tilde{\varphi}, \sin\varphi_m). \tag{31}$$

Here

$$\sin\tilde{\varphi} = \sin\varphi/\sin\varphi_m,$$

$\xi_{electr} = (4\pi K_3 E^2/|\varepsilon_a|)^{1/2}$ is the electric coherence length, $F(\tilde{\varphi}, \tilde{k})$ is the incomplete elliptic integral of the first kind and $\varphi_m = \varphi(D/2)$. Using relationship (31) to change the variable in the integral (4), we arrive at the formula

$$\delta = \left(\frac{2\pi n_o D}{\lambda_{light}}\right) \frac{1}{F(\pi/2, \sin\varphi_m)} \int_0^{\varphi_m} \left[n_e^2 (n_e^2 \cos^2 t + n_o^2 \sin^2 t)^{-1/2} - 1 \right]$$

$$\times (\sin^2\varphi_m - \sin^2 t)^{-1/2}\, dt, \tag{32}$$

which yields the value of birefringence at given electric field-strength E or voltage $\tilde{V}$.

In Figure 5 are presented the theoretical and experimental dependences $\delta(\tilde{V})$ corresponding to two Fredericksz transitions—in a pure nematic and in FN. As the experiments have shown, in thermotropic suspensions $\tilde{E}_c$ is smaller than the corre-

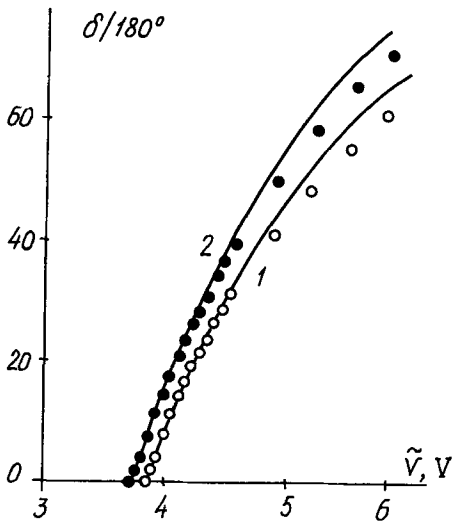

FIGURE 5 Electric voltage dependence of birefringence above the threshold of the dielectric Fredericksz transition for a pure nematic (curve *1*, $D = 222\,\mu$m, $K_3 = 6.74 \cdot 10^{-7}$ dyn) and MBBA-based ferronematic (curve *2*, $D = 240\,\mu$m, $\tilde{K}_3 = 6.37 \cdot 10^{-7}$ dyn). The lines–calculations by Equation (32), the dots–experimental data by Ref. [3,4].

sponding value E_c in undoped nematics. This effect could be accounted for the existence of large aggregates comprising a great number of particles. Around such objects the macroscopic director distortions must have been formed which serve as the pre-existing nuclei of the orientationally-deformed state thus favoring the diminution of the transition threshold. In Ref. [3] on the basis of the obtained critical field $\tilde{E}_c$ the effective value of K_3 has been deduced as $\tilde{K}_3 = D|\varepsilon_a|\tilde{E}_c^2/4\pi^3$. At $\varepsilon_a = -0.5$ the found value had turned out to be $\tilde{K}_3 = 6.37 \cdot 10^{-7}$ dyn, that is approximately 5% lower than the elasticity modulus $K_3 = 6.74 \cdot 10^{-7}$ dyn for pure MBBA. The carried out calculations of $\delta(\tilde{V})$ curves for the corresponding Frank constants are in good agreement with the observed data both for undoped MBBA and FN.

3 BIREFRINGENCE OF A PLANE FERRONEMATIC CELL IN THE CROSSED MAGNETIC AND ELECTRIC FIELDS

3.1 The set of equilibrium equations

Now, having accumulated all the necessary background, we proceed to the theoretical description of the experiments of Refs. [3, 4] on the birefringence of FN subjected to a combination of electric and magnetic fields. The geometry of the cell resembles that of Figure 1 save that now the electric field is imposed along the z-axis. In the initial state FN is a single liquid-crystalline domain ($\boldsymbol{n}_0 = \text{const}$), all over which the magnetization $\boldsymbol{M}_0 = M_s \bar{f}$ is perpendicular to the director. The external magnetic field $\boldsymbol{H}$, inducing the particle rotation and, hence, the rearrangement of the orientational texture, creates in the sample a certain preliminary distortion—see Sec. **1**. The electric field $\boldsymbol{E} = (0, 0, E)$, that acts explicitly on the liquid-crystalline matrix, enhances this distortion tending to rotate the director perpendicular to its initial alignment. In the papers[3,4] a family of the experimental dependences $\delta(\tilde{V})$ for the magnetic field range 1–5 Oe had been measured.

Note that in the presence of the magnetic field $\boldsymbol{H} \perp \boldsymbol{M}_0$ the equilibrium state of the deformed texture corresponds to the perturbations of $\boldsymbol{n}$ and $\boldsymbol{m}$ lying in the plane xOz–see Figure 1. From the bonding conditions (Sec. **6** of Ref. [1]) it follows, that vectors $\boldsymbol{n}$, $\boldsymbol{m}$ and $\boldsymbol{H}_p$ should be coplanar; here $\boldsymbol{H}_p = \boldsymbol{H}_b + \boldsymbol{H}$ is the resulting magnetic field whose direction is tilted relatively to the vertical axis z.

Writing down the orientational distributions $\boldsymbol{n}(z)$ and $\boldsymbol{m}(z)$ in the form (3), we substitute them into Equation (5) extended by adding the electrical term (22). The obtained free-energy functional reads:

$$\mathscr{F} = \int_{-D/2}^{D/2} dz \left[1/2\ K_3 \varphi'^2 (1 + p \sin^2\varphi) - M_s f (H_b \cos\psi + H \sin\psi) + \left(\frac{fW}{d}\right) \sin^2(\psi - \varphi) \right.$$

$$\left. + \left(\frac{f k_B T}{v}\right) \ln f + \frac{|\varepsilon_a|}{8\pi} E^2 \cos^2\varphi \right] \tag{33}$$

Variation of $\mathscr{F}$ with respect to φ, ψ and f yields the set of the equilibrium equations to determine the orientational and concentration distributions $\varphi(z)$, $\psi(z)$ and $f(z)$ for given values of the electric and magnetic field-strengths. After transformations similar to those made for Equations (6)–(18), we arrive at the closed set of four equations:

$$D/2\lambda = Q^{-1/2} I(\varphi_m), \tag{34}$$

$$Q = I(\varphi_m)/J(\varphi_m), \tag{35}$$

$$1 - 2z/D = I(\varphi)/I(\varphi_m), \tag{36}$$

$$\rho\cos\psi - \rho_b \sin\psi = \sigma \sin 2(\psi - \varphi). \tag{37}$$

Here the integrals I and J are defined as follows:

$$I(\varphi) = \int_0^{\varphi} (1 + p\sin^2 t)^{1/2} \left\{ Q[\mathscr{E}(\psi_m, \varphi_m) - \mathscr{E}(\psi(t), t)] + \zeta\left(\sin^2\varphi_m - \sin^2 t\right)\right\}^{-1/2} dt,$$

$$J(\varphi) = \int_0^{\varphi} (1 + p\sin^2 t)^{1/2}\, \mathscr{E}(\psi(t), t) \left\{ Q[\mathscr{E}(\psi_m, \varphi_m) - \mathscr{E}(\psi(t), t)] + \zeta\left(\sin^2\varphi_m - \sin^2 t\right)\right\}^{-1/2} dt,$$

and the parameter $\zeta = |\mathscr{E}_a| E^2 v/8\pi \bar{f} k_B T$ is introduced to characterize the strength of the external electric field; for other parameters the notations of Sec. **1** hold.

The optical response of the system to the applied fields obtained by substitution of Equation (36) into the integral (4) takes the form

$$\delta = \left(\frac{2\pi D n_o}{\lambda_{light}}\right) \frac{1}{I(\varphi_m)} \int_0^{\varphi_m} \left[n_e^2 (n_e^2 \cos^2 t + n_o^2 \sin^2 t)^{-1/2} - 1 \right] (1 + p\sin^2 t)^{1/2}$$

$$\times \left\{ Q[\mathscr{E}(\psi_m, \varphi_m) - \mathscr{E}(\psi(t), t)] + \zeta\left(\sin^2\varphi_m - \sin^2 t\right)\right\}^{-1/2} dt, \tag{38}$$

3.2 Orientation and concentration distributions inside the ferronematic cell. Comparison with the experiment

The initial parts of the theoretical and experimental (taken from Ref. [4]) curves $\delta^{1/2}(\tilde{V}^2)$ at $H = 1.5$, 4.0, 5.0 Oe are presented in Figure 6; the global view of the dependence $\delta(\tilde{V})$ for $H = 2$ Oe is shown in Figure 7. The calculations have been carried out via formulae (34)–(38) in the single-constant approximation with the effective elasticity modulus $K = K_3 = 6.37 \cdot 10^{-7}$ dyn, as in Ref. [3]. The concentration of single-domain grains $\bar{f} = 2.5 \cdot 10^{-7}$ has been determined by comparison of the initial

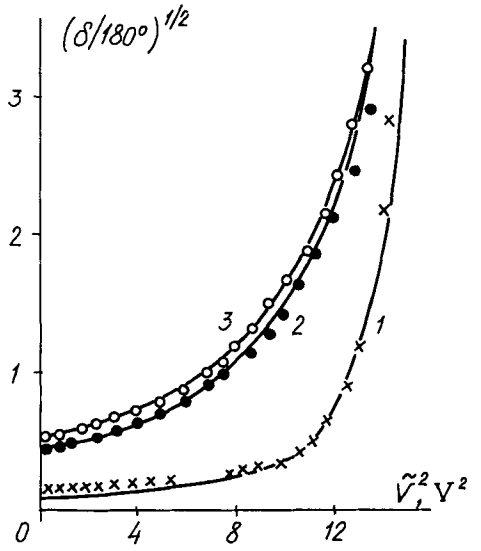

FIGURE 6 Initial parts of the voltage dependences of the electric-induced birefringence for given field-strength H and cell thickness D. The lines–calculations by Equations (34)–(38), the dots-experimental data by Ref. [3]; $H = 1.5$ Oe and $D = 222\,\mu$m–(curve *1* and crosses), 4.0 Oe and 249 μm–(*2* and black circles), 5.0 Oe and 234 μm–(*3* and empty circles).

theoretical and experimental values of $\delta(\tilde{V} = 0)$. Note that the total solid phase content given in Ref. [3,4] was $1.89 \cdot 10^{-6}$.

Let us firstly consider the FN behavior in weak electric and magnetic fields. Solving Equations (34)–(37) under assumptions $\rho\varphi_m \ll 1$ and $\zeta\varphi_m^2 \ll 1$, one gets the following

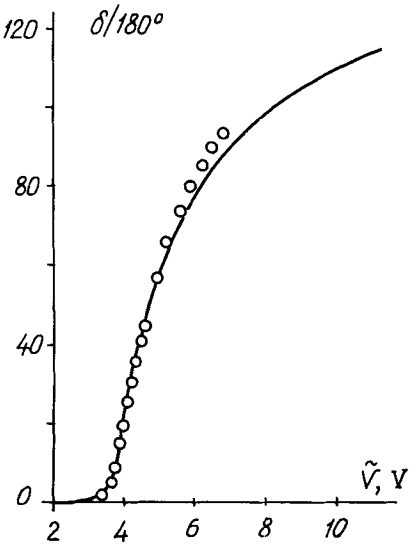

FIGURE 7 Voltage dependence of the electric-induced birefringence for magnetic field strength $H = 2.0$ Oe and cell thickness $D = 230\,\mu$m. The line–calculation by Equations (34)–(38), the dots–experiment by Ref. [4].

expressions for the orientation and concentration profiles

$$\varphi(z)=\frac{M_s\bar{f}H}{8K_3}\left(1+\frac{|\varepsilon_a|E^2D^2}{32\pi K_3}\right)(D^2-4z^2);$$

$$f(z)=\bar{f}\,[1+\rho^2D^2(1+\zeta/8\lambda^2)(1-12z^2/D^2)/48\lambda^2].$$

Substitution of $\varphi(z)$ into the integral (38) gives the optical response in the form

$$\delta=\left[\frac{\pi(n_e-n_o)D^5}{60\lambda_{light}}\right]\left(\frac{M_s\bar{f}H}{K_3}\right)^2\left(1+\frac{|\varepsilon_a|E^2D^2}{32\pi K^3}\right)^2.$$

This expression, duly rescaled, has been used to describe the initial slopes of $\delta^{1/2}(\tilde{V}^2)$.

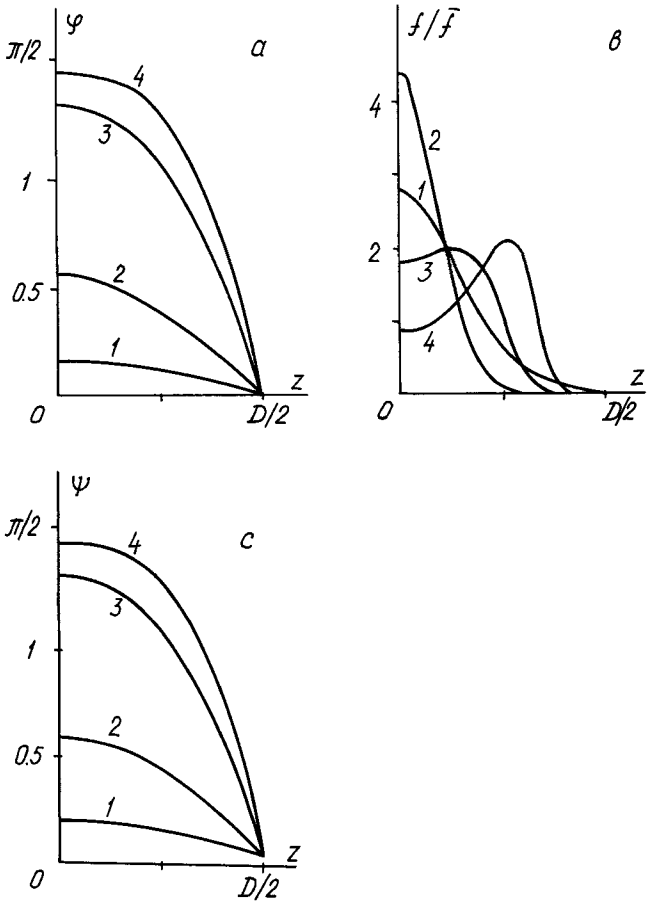

FIGURE 8 Orientation and concentration distributions in FN calculated by Equations (34)–(37) for $H = 2.0$ Oe and $D = 230$ μm. The electric voltage $\tilde{V}$ is 3.7 V(curves *1*), 4.0 V(*2*), 7.0 V(*3*), 11.0 V(*4*).

As the field-strength grows, the seggregation effect begins to play an important part in formation of the equilibrium texture. With the increase of the magnetic field, the particles gather in the middle section of the cell intensifying the director tilt there. The applied electric field enhances this orientational deformation and also influence the particle distribution. These effects are illustrated by the curves in Figure 8 calculated with the aid of Equations (34)–(37). One sees that as $\tilde{V}=ED$ raise, the particle concentration in the centre of the cell begins to grow and reaches the maximum at $\tilde{V}\approx 4\,V$. Further on, when the electric field causes substantial deformations of the orientational texture, the opposite tendency steps in—ferroparticles leave the central part of the cell and accumulate in those regions, where the conditions $\boldsymbol{m}\perp\boldsymbol{n}$ and $\boldsymbol{m}\parallel\boldsymbol{H}_p$ of their minimum energy are favored. Due to that the concentration profile of FN changes. In the centre of the cell the minimum of $f(z)$ occurs and, instead of one maximum, two of them at equal distances from the middle, turn up—see curves *3*, *4* in Figure 8. Apparently, the particle re-distribution affects the orientational profile $\varphi(z)$ and, hence, the birefringence δ.

It is important to emphasize that the correct interpretation of the experiment is impossible if the seggregation effect is ignored. Having not taken it into account, the authors of Refs. [3,4] had been compelled to introduce (though lacking physical reasons) a strong dependence of the elastic modulus of the liquid-crystalline matrix upon the applied magnetic field strength. The direct attempt to fit the experimental points in the non-seggregation approximation has lead them to the following values (cf. the legend to Fig. 6)

H,[Oe]	0	1.5	4.0	5.0
$\tilde{K}_3(H)$,[$\times 10^{-7}$ dyn]	6.4	5.8	5.1	4.8

In fact, our consideration proves—see also Figures 7,8—that the assumed function $\tilde{K}_3(H)$ is an artifact. The value of the elastic modulus K_3, once modified by the presence of the solid admixture, does not need to be changed in any field, providing the seggregation is taken into account.

CONCLUSIONS

The above-presented theoretical review of the behavior of thermotropic FN demonstrates that the surface interactions on the liquid crystal—particle interface affect substantially the orientational, magnetic and optical properties of these media. The developed in Ref. [1] and herein model, that takes into account these interactions, is capable to provide a non-contradictory interpretation, previously absent, of the existing experimental data. As to the latter, however, on close inspection one becomes aware that there is a great need in the properly defined schemes to evaluate the material parameters of FN. The most essential ones of them are: the effective Frank moduli K_i, the amplitude W of the anchoring energy and the really achieved concentration $\bar{f}$ of single-domain magnetic grains.

On the basis of our results the following way to determine the material parameters of FN may be proposed.

- By the critical value of the potential difference $\tilde{V}_c = \tilde{E}_c D$ of the Fredericksz transition in the electric field the effective moduli K_2 and K_3 are found. Indeed, as it is shown in Sec. **2**, for the homeotropic texture of FN the value of $\tilde{E}_c$ depends solely on K_3 and for the planar one—only on K_2.
- Concentration of the single-domain grains $\bar{f}$ could be deduced from the initial slope of the optical response $\delta^{1/2}(H)$, as it has been done with the curves of Figures 2, 3.
- The values of the anchoring energy W and the effective modulus K_1 could be evaluated by the critical field strength $\tilde{H}_c$ that corresponds to the magnetic Fredericksz transition in a strong bias field.

Acknowledgement

This work was done partially under the auspices of the International Science Foundation under the grant No. RMD 000 of the Long-Term Research Grant Program.

References

1. Burylov, S. V., and Raikher, Yu. L., Part I of this paper.
2. Chen, S.-H., and Amer, N. M., *Phys. Rev. Lett.*, **51**, 2298 (1983).
3. Chen, S.-H., Liang, B. J., *Optics Lett.*, **13**, 716 (1988).
4. Liang, B. J., Chen, S.-H., *Phys. Rev. A*, **39**, 1441 (1989).
5. Burylov, S. V., and Raikher, Yu. L., *Phys. Lett. A*, **149**, 279 (1990).
6. Burylov, S. V., and Raikher Yu. L., *J. Magn. and Magn. Mater.*, **122**, 62 (1993).
7. Raikher Yu. L., Burylov, S. V., and Zakhlevnykh, A. N., *Sov. Phys.-JETP*, **64**, 319 (1986).
8. Brochard, F., and de Gennes, P. G., *J. Phys.* (France), **31**, 691 (1970).
9. de Gennes, P. G., *The Physics of Liquid Crystals* (Clarendon Press) (1974).
10. Pieranski, P., Brochard, F., and Guyon, E., *J. Phys.* (France), **34**, 35 (1973).